Structural characterization of the interaction of α-synuclein nascent chains with the ribosomal surface and trigger factor

Annika Deckert[1], Christopher A. Waudby[1], Tomasz Wlodarski[1], Anne S. Wentink[1], Xiaolin Wang[1], John P. Kirkpatrick[1], Jack F. S. Paton[1], Carlo Camilloni[2], Predrag Kukic[2], Christopher M. Dobson[2], Michele Vendruscolo[2], Lisa D. Cabrita[1] & John Christodoulou[1]

[1]Institute of Structural and Molecular Biology, University College London, London, UK
[2]Department of Chemistry, University of Cambridge, Cambridge, UK
Correspondence to:j.christodoulou@ucl.ac.uk

The ribosome is increasingly recognized as a key hub for integrating quality control processes associated with protein biosynthesis and co-translational folding(CTF). The molecular mechanisms by which these processes take place, however, remain largely unknown, in particular in the case of intrinsically disordered proteins(IDPs). To address this question, we studied at a residue-specific level the structure and dynamics of ribosome-nascent chain complexes(RNCs) of α-synuclein(αSyn), an IDP associated with Parkinson's disease(PD). Using solution-state nuclear magnetic resonance(NMR) spectroscopy and coarse-grained molecular dynamics(MD) simulations, we find that, although the nascent chain(NC) has a highly disordered conformation, its N-terminal region(NTR) shows resonance broadening consistent with interactions involving specific regions of the ribosome surface. We also investigated the effects of the ribosome-associated molecular chaperone trigger factor(TF) on αSyn structure and dynamics using resonance broadening to define a footprint of the TF-RNC interactions. We used these data to construct structural models that suggest specific manners by which emerging NCs can interact with components of the biosynthesis and quality control machinery.

Protein biosynthesis is carried out by ribosomes, the macromolecular machines present in all kingdoms of life. Aided by molecular chaperones, nascent proteins can begin to fold while emerging from the ribosome. Achieving their native fold, and avoiding misfolding, is thereby crucial for the fate of all nascent proteins. The molecular details of this fundamental process,

however, are poorly understood. In this work we develop a combined NMR and molecular simulation approach to characterize the behavior during biosynthesis of αSyn, an IDP associated with PD. The detailed interactions of αSyn with the ribosome surface and TF, a ribosome-associated chaperone, reveal the first steps of how a NC emerges from the ribosome.

Within living systems, protein biosynthesis takes place at the peptidyl transferase centre(PTC) of the ribosome, where peptide bond formation occurs at a rate of ~20amino acids/second[1] to generate a nascent polypeptide chain(NC) that subsequently emerges through the exit tunnel[2], a ~100Å passage which can accommodate ca. 30 residues[3]. On emerging from the tunnel NCs can begin to explore their conformational landscapes, where about a third of cytosolic proteins in *E.coli* are expected to acquire native-like structure co-translationally[4,5]. CTF may, therefore, be a key process to assist NCs in adopting their native folds by minimizing the exposure of hydrophobic regions and reducing the risk of misfolding and aggregation[6,7].

To ensure the production of correctly folded and functionally active proteins, further mechanisms have evolved to regulate folding pathways. Evidence indicates that the ribosome itself can modulate the folding process[8] by reducing the rate of tertiary contact formation and inhibit misfolding by stabilizing unfolded states[9]. Fluorescence depolarization measurements have also shown that the dynamics of emerging NCs can be constrained[10], particularly those of a positive charge[11], owing to interactions with the negatively charged ribosome surface, which are said to create a protective environment within the crowded cell[12].

CTF processes within the cell can also be modulated by chaperones[13]. In *E.coli,* the first chaperone encountered by an emerging NC is TF, which binds transiently to the ribosome via a docking site on L23[14,15], forming a cradle above the exit tunnel. It has been proposed that TF promotes CTF in several ways, including by shielding exposed hydrophobic stretches[16], inhibiting premature folding[17], and by unfolding pre-existing structures and intermediate states[8]. TF binds to untranslating ribosomes with a K_d of ca. 1μM[18], but this affinity can be significantly stronger in the presence of NCs(depending on their sequences[19] and lengths[20]). TF comprises three distinct structural regions: an N-terminal ribosome-binding domain(RBD), a peptidyl-prolyl isomerase domain(PPD) and a centrally located, C-terminal substrate-binding domain(SBD). An NMR study of interactions of free TF with isolated, unfolded PhoA[21] identified four binding sites within TF, of which three are located within the SBD and one in the PPD. The

regions of PhoA that interacted most strongly with these sites were found to be rich in hydrophobic and aromatic residues, in accord with the known substrate preferences of TF[19].

Although structural studies of CTF are still few, solution-state NMR of translationally-arrested NCs is emerging as a powerful means of reporting high resolution details[22-24], despite the high molecular weight(2.5MDa) of RNCs[25], the low working concentrations(~10μM), and their limited lifetimes. Furthermore, computational approaches based on MD simulations have also been developed to investigate the nature and properties of CTF[26,27] processes, although the large size of the ribosome and relatively slow rates of protein synthesis and folding still pose major challenges for all-atom calculations on appropriate timescales. To circumvent this problem, coarse-grained methods have been adopted to allow the inherent properties of a system to be preserved while using a reduced molecular representation to minimize the number of elements in the simulations[28].

Here we show that combined NMR and MD studies of RNCs of αSyn, a protein whose aggregation is associated with PD, can provide insight into the conformations sampled by a disordered polypeptide chain during synthesis, complementing information emerging from studies of the CTF of globular proteins, as well as existing structural descriptions of αSyn that have been obtained for the protein in isolation[29] and within cells[30,31].

RESULTS

αSyn is disordered on the ribosome

αSyn RNCs, translationally arrested using the SecM motif[32], were generated in *E.coli*(**Fig.1a**), and the samples were purified based on our previous method[33], with the removal of the N-terminal His(H_6)-tag using TEV protease(**Fig.S1a,b**). ^{1}H-^{15}N SOFAST-HMQC[34] spectra with non-uniform weighted sampling(NUWS) sensitivity enhancement[35] were acquired(**Fig.1b**) alongside biochemical analyses[36]**(Fig.1f**&**Fig.S1c-f)** and ^{15}N-XSTE diffusion measurements[37]**(Fig.S1g-i)** to monitor the integrity of the RNC, which showed that the NC was attached and that the samples remained essentially completely stable for ~72h.

The ^{1}H-^{15}N NMR correlation spectrum of the αSyn RNC(**Fig. 1b**) shows a narrow range(8–8.8ppm) of amide proton chemical shifts(CS) characteristic of an IDP, and overlays closely with a matching spectrum of isolated αSyn in the presence of an equimolar

concentration of 70S(**Fig.1c,d**&**Fig.S2b**). CS differences were uniformly small ($\Delta\delta_{NH}$<0.05ppm,**Fig.S3a**), indicating that the NC samples a range of disordered state conformations similar to isolated αSyn, which allowed the transfer of cross-peak assignments to that of the RNC**(Fig. 1b)**. Due to line broadening and overlap in the RNC spectrum, 63 αSyn resonances, from M5-D135, were resolved sufficiently to enable their intensities to be analyzed. Critically, the observation of the D135 resonance(**Fig.1b,e**), located just 28 residues from the PTC, indicates that the NC possesses extensive mobility near the opening of the exit tunnel, which accommodates ca. 30 residues[3].

Resonance broadening indicates interactions of αSyn with the ribosome surface

In contrast to the minimal CS perturbations observed in the NC, large reductions in the intensities of NC resonances were observed relative to those of isolated αSyn(**Fig.1d,e**). This effect provides a sensitive probe of the changes in NC dynamics associated with the gain in mobility of the polypeptide chain as it emerges from the exit tunnel, and with the loss of mobility arising from interactions with the ribosome surface.

The intensities of cross-peaks in the RNC spectrum were reduced by >87% relative to isolated αSyn in the presence of ribosomes, with substantial variation across the sequence(**Fig.1e**). The C-terminal resonances were highly broadened, but from residue D135-K58 resonances were generally observed to become narrower(and hence more intense), indicating that NC mobility is increased as residues become more distant from the exit tunnel. However, from K58 to the N-terminus this trend is reversed as resonances are progressively broadened, with decreased intensities. These results indicate an increasing propensity of this region to interact with the ribosome surface, which appears to be correlated with a high density of positively charged residues. In contrast, the negatively charged C-terminal region(CTR) remains observable, despite its increased proximity to the ribosome surface. In addition to these long-range trends, two clusters of residues, M5–S9 & V37–V40, were broadened beyond detection, while intensities in a third region centered around T92/G93 were attenuated to a lesser extent. These clusters appear to be associated with the aromatic residues F4,Y39&F94, rather than generally with hydrophobicity as the most hydrophobic region of the sequence, N65–T75, is also the region of greatest intensity.

For comparison, we also examined changes in the intensity of isolated αSyn in the presence of ribosomes. Reductions in intensity of up to 60–70% were observed for N-terminal

residues(M5,L8,S9), without any perturbations to the CTR(**Fig.S2c**). This broadening of N-terminal resonances is comparable to that observed in the αSyn RNC, suggesting that similar interactions occur with the ribosomal surface in both cases, although the effect is substantially weaker in the absence of the covalent tethering in the RNC. Further analyses of charged isolated αSyn variants suggested that the polypeptide-70S interactions are at least in part due to electrostatic interactions**(Fig.S5)**.

To probe the dynamics of the NC in more detail, ^{1}H linewidths were measured in spectra of the RNC and isolated αSyn(**Fig.2a**&**Fig.S3b**). RNC resonances were found to have significantly larger linewidths(and hence R_2 relaxation rates) than those in isolated αSyn, with an increase in R_2 from 37±7 s^{-1}(mean±s.d.) for the isolated protein to 109±38 s^{-1} in the RNC(**Fig.2b**). To determine the significance of such values, we estimated the R_2 values that might be expected for a NC immobilised by tight binding to the ribosome surface. ^{1}H-^{1}H dipolar interactions were calculated using an ensemble model of the αSyn RNC(see below), taking the rotational correlation time of the ribosome to be 3.9μs at 277K[38], from which we estimate the amide proton relaxation rates of the bound state to be 16.1±4.4×10^{3} s^{-1}(**Fig.S3c**). Using this estimate, and making the assumption that NC resonances are in fast exchange between free and ribosome-associated states, as is typically the case for weak interactions, the observed relaxation rates will be a population-weighted average of the free and bound states[24]. Thus using the observed linewidths of residues between V48 & A124(**Fig.2b**), the estimated population of this NC segment bound to the ribosome surface is 0.45±0.24%(**Fig. S3d**). While this number could be increased if the bound state were to be significantly mobile(**Fig.2c**), this analysis nevertheless indicates that these interactions are of a weak and transient nature. It is likely that interactions with the ribosome surface for other segments of the NC, whose resonances are more severely broadened and so cannot be observed(**Fig.1e**), could be considerably stronger.

NMR analysis of trigger factor-nascent chain interactions

In order to examine the impact of a ribosome-associated chaperone on the behavior of the αSyn NC, [^{2}H,$^{13}CH_3$-ILV]-labeled TF was titrated into a ^{15}N-labeled sample of αSyn RNC. While ribosome-bound αSyn has been shown to be a weak substrate for TF[39,40], TF itself has a moderate affinity for untranslating 70S ribosomes(K_d ~1μM[18]). This combination of affinities was important in allowing saturation of the NC-TF interaction without the complication of

strong NC binding causing substantial line-broadening. We found that the addition of 1 mol. equiv. of TF induced only small amide CS perturbations($\Delta\delta_{NH}$<0.06ppm,**Fig.3a**&**Fig.S4a**) indicating that the NC samples a similar distribution of disordered conformations as it does in the absence of TF. We observed, however, large and non-uniform reductions in the intensities of the αSyn cross-peaks(**Fig.3b**), which enabled the nature of the TF-NC interaction to be analyzed. The intensities of residues K21-G111 in the RNC spectrum were reduced to 30±8% of those observed in the absence of TF, while resonances of residues D119-D135 in the CTR were less strongly perturbed, with relative intensities reduced only to 88±12%(**Fig.3b**). No effects on the resonances of residues N-terminal to K21 could be determined, as these resonances are already broadened beyond detection in the absence of TF(**Fig. 1e**). The addition of TF concentrations higher than 1 mol. equiv. caused no further intensity changes in the RNC spectrum indicating that, although the TF-NC interaction may be weak, the TF-70S interaction itself had reached saturation(**Fig.3c**).

Analysis of the $^{1}H,^{13}C$ spectrum of TF showed that methyl resonances experienced large reductions in intensity in the presence of ribosomes(~6-fold reduction relative to isolated TF,**Fig.S4d**), but little additional broadening was observed in the presence of the αSyn NC(**Fig.3d**), which is consistent with previous observations using fluorescence techniques that showed no increased recruitment of TF to ribosomes carrying an αSyn NC[40]. For comparison, we examined changes in the spectrum of isolated αSyn in the presence of 1 mol. equiv. of TF. At concentrations of 5μM only small intensity changes(<5%) were observed, in residues located at the N-terminus of αSyn. However, additional line broadening was evident at higher concentrations(100μM), or in the presence of ribosomes(which promote the dissociation of the TF dimer)(**Fig.S4c**). Thus, while αSyn is indeed a weak TF substrate there is nevertheless some propensity to interact, and this may be promoted by the ribosome and, particularly, by the co-localization of TF and the NC during translation.

Structural modeling of the αSyn RNC

Coarse-grained simulations of the αSyn RNC were used to develop a model with which to explore the structure and dynamics of the NC and to investigate potential sources of the NMR resonance broadenings observed. Here, we used the CamTube force field[41], in which the polypeptide chain is represented as a flexible tube as a means of describing its overall architecture. This approach increases the efficiency of sampling protein conformations relative

to all atom simulations, making it particularly effective for the study of large and flexible systems such as RNCs. Starting structures for the simulations were constructed from cryo-EM models of SecM-stalled translating ribosomes, where the 17-residue arrest sequence has an extended conformation in the exit tunnel[42], and structural ensembles for the NC were then generated from a 2.4μs trajectory(**Fig.4a**&**VideoS1**). From this ensemble, we found that the first NC residue to be located in the exit vestibule was D135, 28 residues (78Å) from the PTC. Critically, this point coincides with the experimental observation of NC resonances, and the subsequent increase in intensity from D135 towards the N-terminus(**Fig.1e**). To estimate the rotational mobility of each residue within the NC, the structural ensemble was used to calculate S^2 order parameters, where a value of 1 describes rigid residues, and a value of 0 describes fully flexible residues. We found that the observed increase in NMR intensities from D135-E104(**Fig.1e**) was associated with a decrease by two orders of magnitude in the calculated amide S^2 values(**Fig.4c**), as well as a large increase in mobility as described by the Cα root mean square fluctuations (RMSF)(**Fig.4d**). However, both parameters also predict a continued gain in mobility for residues more distant from the PTC, whereas the NMR data showed reduced peak intensities for residues in the vicinity of T92/G93 and for the NTR (M5–V40)(**Fig.1e**). We thus conclude that the observed perturbations in NMR peak intensity are the likely consequence of a combination of electrostatic effects induced by positively charged residues in the N-terminus and interactions with aromatic residues(F4/Y39/F94).

The simulations were repeated in the presence of ribosome-bound TF, using a starting structure based on an NMR model of TF in complex with the disordered state of PhoA[21](**Fig.4b**&**Video S2**). We observed that the αSyn residues K21–G111, which experienced the strongest reduction in resonance intensities on TF binding(~70%)(**Fig.3b**), were able to contact proposed substrate binding sites in TF previously identified in the absence of the ribosome[21]. Conversely, we found that the C-terminal residues D119-D135, which were only marginally broadened(~12%) upon TF binding, were not able to contact sites within TF. Interestingly, reductions in Cα RMSF values and S^2 order parameters were observed in the presence of TF for residues between E126 and the N-terminus(**Fig.4c,d**). However, no TF-induced perturbations in NMR signal intensities were observed experimentally in the vicinity of E126 (**Fig.3b**), suggesting that TF interactions do not occur within this region. Thus, while our modeling suggests that a restriction in mobility could be experienced from residues from E126,

the NMR data show interactions of the NC and TF appear only to occur from residues G111, presumably when these can begin to reach and interact with the TF cradle(**Fig.4b**).

Using the simulated RNC structures we identified ribosomal proteins accessible to the NC, and also mapped the changes in NC accessibility of the ribosome surface that occur upon TF binding. **Fig.4e** illustrates the accessibility of the ribosome surface for the NC, which was calculated as the distance of closest approach between the backbone atoms of the NC and atoms of the 70S surface. Regions close to the exit tunnel, which are within 10Å of the NC(in red), include the ribosomal proteins L17,L22&L32, which are important binding sites for protein biogenesis factors[43] such as peptide deformylase(PDF) and methionine aminopeptidase(MAP), as well as L23,L24,L29,L32&rRNA. Upon binding of TF, the NC formed additional contacts with the chaperone at the expense of other regions of the ribosome surface, which became sterically occluded(**Fig.4f**). **Fig.4g** indicates the changes of the NC surface accessibility in the presence and absence of TF(compare **Fig.4e**&**4f**). Regions corresponding to the ribosomal proteins L3,L17,L19,L22&L32(blue) became inaccessible upon binding of TF but as a consequence other regions(in red), including L4&L28 as well as parts of L9&L24 were sampled more often by the NC(**Fig.4h**).

DISCUSSION

We have used high-resolution solution NMR and coarse-grained MD to characterize the structure, dynamics and interactions of αSyn NCs during biosynthesis on the ribosome. The limited solubility of RNC samples together with the observed NMR line broadening resulted in very weak signal intensities, equivalent to just 50–100nM concentrations of isolated αSyn. Nevertheless, a combination of methodological advances, including longitudinal relaxation optimized experiments and non-uniform weighted sampling[34,35], have enabled quantitative measurements to be made of CSs and cross-peak intensities for the majority of NC residues. Most importantly, a combination of biochemical and non-invasive spectroscopic assays were applied to ensure that all NMR signals analyzed in this study arise from intact, ribosome-bound NCs(**Fig.1f**&**Fig.S1g-i**).

Previous RNC structural studies have focused almost exclusively on examining folding competent globular proteins such as ddFLN5[22], SH3[24] domains & barnase[23]. In contrast to folded

states, which correspond to deep minima in free energy landscapes, IDPs have relatively flat free energy landscapes[44] that are highly sensitive to external perturbations, e.g., from mutations[45], posttranslational modifications[46] or from the intracellular environment[47]. The investigation of IDPs therefore allows a detailed exploration of the accessible conformational space for a polypeptide chain, without complications of folding.

NMR CSs are typically sensitive probes of protein structure, yet we found that αSyn amide CS perturbations resulting from ribosomal attachment, or from the presence of TF, were extremely small(**Fig.S3a**&**FigS.4a,b**). By contrast, the intensities of cross-peaks in spectra of the RNC were highly variable relative to isolated αSyn(**Fig.1d,e**). The tethered motion of the NC inevitably affects NMR linewidths, given the thousand-fold difference in the effective rotational correlation times of the ribosome and of isolated αSyn. Residues will therefore generally gain independent mobility as they become more distant from the PTC and emerge from the exit tunnel. In this study, the residue closest in sequence to the PTC to be NMR detectable was D135, from which point resonance intensities increased to a maximum at K58(**Fig.1e**). Our structural modeling indicated that the position of D135, 28 residues from the PTC, coincides with the emergence of the NC from the constricted tunnel into the exit port(**Fig.4a**). The detection of these resonances therefore demonstrates the potential to structurally dissect the behavior of NCs that are close to, and potentially even within, the exit vestibule.

Further from the PTC, from residues K58-M5, our simulations indicate that the mobility of each residue continues to increase(**Fig.4c,d**). We observed, however, that the intensities of NC resonances in this region were significantly less than those of residues closer to the PTC. In particular, clusters of resonances in the NTR, encompassing M5–S9 & V37–V40, were broadened beyond detection as well as resonances around T92/G93, which showed a significant(~97%) attenuation in NMR signal(**Fig.1e**), indicating the existence of interactions between the NC and the ribosome surface. Interestingly, the line broadening observed in the NTR of the RNC was also observed for isolated αSyn in the presence of ribosomes(**Fig.S2c**), suggesting a similar mode of interaction, although substantially weaker in the absence of a covalent link to the ribosome. Such interactions have previously been observed for RNCs, by NMR for ddFLN5[22] and SH3[24], by fluorescence methods for the IDP PIR[11], and by optical force spectroscopy for T4 lysozyme[9]. In the latter two cases, interactions were driven at least partially by the high negative charge density of the ribosome surface, and modulations of the electrostatic

environment by ionic strength[9] or differently charged variants of the NC[11] were shown to perturb the binding interaction. In the present study, the large number of resolved NC resonances provided us with the ability to unravel sequence determinants of these interactions, from the identification of αSyn residues interacting with the ribosome surface. We conclude that the net positive charge of the NTR(resulting from the αSyn KTKEGV repeat motif) induces electrostatic interactions with the ribosome surface, which in isolation are reduced in the reverse-charged K6-60E αSyn variant, in which positive charges are eliminated, or increased in the more positively charged H_6-tagged αSyn**(Fig.S5)**. We also observed that interactions of the clusters around M5-S9, V37-V40 & T92-G93 are associated with the aromatic residues F4,Y39&F94**(Fig.1e)**. As the interaction pattern does not correlate with the known region of hydrophobicity within αSyn**(Fig. 1e)**, this indicates that there may be a specific affinity of the ribosome surface for aromatic residues. Interestingly, similar patterns of NMR line broadening have been observed for αSyn within bacterial[31] and mammalian cells[48], which suggests that there may be a common role for charged and aromatic residues in governing protein interactions both with the ribosome surface and with other components of the cellular milieu.

NMR intensity analysis provides a sensitive and high-resolution probe of ribosome surface interactions, but due to the interplay of ^{1}H & ^{15}N relaxation processes, their quantitative interpretation in terms of NC dynamics is not currently possible. We therefore also measured ^{1}H linewidths for 31 NC residues from V48-A124, to provide a quantitative estimate of ribosome binding(**Fig.2**&**Fig.S3b-d**). Relaxation rates for the bound state of the NC were evaluated using an ensemble model of the RNC in which the correlation time of the NC was set equal to that of the ribosome(**Fig.S3c**), and on this basis we determined an average bound state population of 0.45±0.25% for residues in this segment of the NC(**Fig.S3d**). While this interaction is rather weak, residues that were unobservable by NMR (M5-S9 & V37-V40) are likely to be interacting more strongly with the ribosome surface. Moreover, as the bound state may represent a set of interconverting states rather than a single rigid conformation, the collective effect of many weak interactions means that the total population of the NC in association with the surface at any given instant may be substantially greater than 0.45%(**Fig.2c**).

Finally, we have reported residue-specific details of the interaction of the ribosome-associated chaperone TF with a NC. Intensity reductions of ~70% were observed for residues K21-G111 of the αSyn RNC in the presence of TF. While this region spans the net positively

charged NTR(K21-E61), the hydrophobic NAC region(Q62-V95), and part of the negatively charged CTR(K96-G111), the observed broadening was found to be approximately uniform and hence independent of the previously identified preferences of TF for basic and hydrophobic substrates[19, 21]. Instead, our structural modelling indicates that the observed broadening can be better correlated with those residues able to reach the TF cradle and its associated binding sites(**Fig.4b**). These NMR data indicate that 52 residues are necessary from the PTC to initiate an interaction with TF, with G111 being the first residue to be significantly perturbed in intensity. Cross-linking studies[49] as well as theoretical calculations based on the crystal structure of ribosome-bound TF[15] have found similar minimum lengths to be necessary for NC-TF contact formation(47&43 residues respectively). The results described here add residue-specific detail to these previous findings, confirming that NC lengths of about 50 residues are required to initiate interactions with TF.

In summary, this study begins to describe the structural and dynamic characteristics of disordered NCs during biosynthesis by examining the behavior of αSyn, an IDP associated with PD and related neurodegenerative conditions. As αSyn is free from competition with CTF processes encountered by globular proteins, this study provides an insight into the earliest events experienced by emerging NCs, prior to the onset of CTF. The results show that the disordered structural ensemble of αSyn is not strongly perturbed when tethered to the ribosome, though with the sensitivity of the NMR measurements it was possible to identify and characterize very weak interactions of the NC with ribosomal proteins near the exit tunnel. Such interactions, mediated by charge and aromatic residues, are also likely to be determining factors that impact on CTF of globular proteins, particularly as the ribosome is associated with having a direct chaperoning capacity[8,9]. Furthermore, although αSyn is a weak TF substrate, we could show that TF interacts with the N-terminal ~110 αSyn residues, including the positively charged NTR, the hydrophobic NAC region as well as unexpectedly residues of the negatively charged CTR. This study shows that even weak substrates, including residues not known to bind TF, are affected by the presence of the chaperone indicating that an interplay exists between the surface of the ribosome and that of the TF cradle upon the immediate exit of a NC from the ribosome. These observations have implications for understanding the CTF process, as the folding of a NC may not only be assisted by interactions with the ribosome surface, but also by the extent of TF involvement, resulting in a complex folding landscape. Such interactions could

thus have a protective role for emerging NCs particularly those likely to possess substantial regions of disorder, by preventing co-translational misfolding induced by non-native intra- or intermolecular interactions during biosynthesis[50].

MATERIALS & METHODS

Detailed Materials & Methods contained in SI.

Preparation of αSyn RNCs. The αSyn gene was cloned into a pLDC-17 vector[33] and site-directed mutagenesis was used to introduce a TEV protease cleavage sequence between the N-terminal H_6-tag and αSyn. Uniformly ^{15}N-labelled RNCs were expressed in *E.coli* and purified as described previously[33]. TEV protease was used to cleave the H_6-tag from the RNCs following nickel affinity chromatography.

Preparation of TF. Isotopically labelled TF, including selective protonation of Ile, Leu and Val methyl side chains was produced in *E.coli* according to standard procedures.

Detection of RNCs. RNC samples collected during purification or NMR acquisition were run on bis-tris polyacrylamide gels(pH 5.8) prior to western blot. Polyclonal rat anti-αSyn(epitope residue 15-123)(BD Laboratories) and polyclonal rabbit anti-SecM(epitope SecM motif) antibodies were used to detect the NC.

NMR spectroscopy. NMR data were acquired at 4°C on a 700MHz Bruker Avance III spectrometer with TXI cryoprobe. ^{1}H-^{15}N SOFAST-HMQC[34] spectra were recorded using non-uniform weighted sampling[35]. ^{15}N XSTE and ^{1}H STE diffusion experiments were acquired using a diffusion delay of 100ms and bipolar trapezoidal gradient pulses (total length 4ms, shape factor 0.9) with strengths of 0.028 and 0.532Tm^{-1}.

Coarse-grained MD simulations of the αSyn RNC. An atomic model of a stalled NC on the ribosome was derived from cryoEM data[42] by molecular-dynamics flexible fitting[51]. To produce an αSyn RNC starting model, the original NC sequence in the model was replaced and extended to the sequence of the αSyn RNC using Swiss-PDB Viewer. TF bound to the ribosome was modeled based on the cryoEM data of the ribosome-TF complex[49] and the structure of TF[14,15]. Simulations of the αSyn RNC were performed in Gromacs[52] using a version of the tube model[41],

known as the CamTube force field using a 2.4μs trajectory. The NC mobility for each residue was calculated as the RMSF from the average position of the CA atoms within the trajectory and amide S^2 generalized order parameters were calculated from an ensemble of 8000 all-atom structures.

ACKNOWLEDGMENTS

We thank B. Bukau (Ruprecht-Karls-University) for the anti-SecM antibody and J. Gumbart (Georgia Institute of Technology) and K. Schulten (University of Illinois) for providing the stalled ribosome-starting structure. J.C. acknowledges the use of the Biomolecular NMR Facility, University College London, and thanks T. Frenkiel and G. Kelly of the Medical Research Council Biomedical NMR Centre at the Crick Institute, London for the use of the facility. J.C. and T.W. acknowledge the use of the Advanced Research Computing High End Resource (ARCHER) UK National supercomputing service (www.archer.ac.uk/). L.D.C. is supported by the Wellcome Trust and by an Alpha-1 Foundation grant. T.W. is supported as a European Molecular Biology Organization Long-Term Fellow and is also supported by the Wellcome Trust. A.D. is supported by the Motor Neurone Disease Association. The work of C.M.D and M.V. is supported by a Wellcome Trust Programme Grant (094425/Z/10/Z to C.M.D. and M.V.). This work was supported by a Biotechnology and Biochem- ical Sciences Research Council New Investigators Award (BBG0156511 to J.C.) and a Wellcome Trust Investigator Award (097806/Z/11/Z to J.C.).

REFERENCES

1. Liang,S.T., Xu,Y.C., Dennis,P. & Bremer,H. mRNA composition and control of bacterial gene expression. *J. Bacteriol.* **182**, 3037-3044 (2000)
2. Bhushan,S. *et al.* α-Helical nascent polypeptide chains visualized within distinct regions of the ribosomal exit tunnel. *NSMB.* **17**, 313-317 (2010)
3. Lu,J. & Deutsch,C. Secondary structure formation of a transmembrane segment in Kv channels. *Biochem.* **44**, 8230-8243 (2005)
4. Ciryam,P., *et al. In vivo* translation rates can substantially delay the cotranslational folding of the *E. coli* cytosolic proteome. *PNAS* **110**, E132-E140 (2013)

5. Zhang,G & Ignatova,Z. Folding at the birth of the nascent chain: coordinating transaltion with co-translational folding. *Curr. Opin. Struc. Biol.* **21**, 25-31 (2011)
6. Dobson,C.M. Protein folding and misfolding. *Nature* **426**, 884-890 (2003)
7. Frydman,J., Erdjument-Bromage,H., Tempst,P. & Hartl,U. Co-translational domain folding as the structural basis for rapid *de novo* folding of firefly luciferase. *NSMB* **6**, 697-705 (1999)
8. Hoffmann,A. *et al.* Concerted action of the ribosome and the associated chaperone trigger factor confines nascent polypeptide folding. *Mol. Cell.* **48**, 63-74 (2012)
9. Kaiser,C.M., Goldman,D.H., Chodera,J.D., Tinoco Jr,I. & Bustamante,C. The ribosome modulates nascent protein folding. *Science* **334**, 1723-1727 (2011)
10. Ellis,R.J., Culviner,P.H. & CavagneroS. Confined dynamics of a ribosome-bound nascent globin: Cone angel analysis of fluorescence depolarization decays in the presence of two local motions. *Prot. Sci* **18**, 2003-2015 (2009)
11. Knight,A.M. *et al.* Electrostatic effect of the ribosomal surface on nascent polypeptide dynamics. *ACS Chem. Biol.* **8**, 1195-1204 (2013)
12. Gershenson,A. & Gierasch,L.M. Protein folding in the cell: challenges and progress. *Curr. Opin. Struct. Biol.* **21**, 32-41 (2011)
13. Preissler,S. & Deuerling,E. Ribosome-associated chaperones as key players in proteostasis. *TiBS.* **37**, 274-283 (2012)
14. Kramer,G. *et al.* L23 protein functions as a chaperone docking site on the ribosome. *Nature* **419**, 171-174 (2002)
15. Ferbitz,L. *et al.* Trigger factor in complex with the ribosome forms a molecular cradle for nascent proteins. *Nature* **431**, 590-595 (2004)
16. Kaiser,C.M. *et al.* Real-time observation of trigger factor function on translating ribosomes. *Nature* **444**, 455-460 (2006)
17. Mashaghi,A. *et al.* Reshaping of the conformational search of a protein by the chaperone trigger factor. *Nature* **500**, 98-101 (2013)
18. Patzelt,H. *et al.* Three-state equilibrium of *E.coli* trigger factor. *Biol. Chem.* **383**, 1611-1619 (2002)
19. Patzelt,H. *et al.* Binding specificity of *E.coli* trigger factor. *PNAS* **98**, 14244-14249 (2001)

20. Raine,A. *et al.* Trigger factor binding to ribosomes with nascent peptide chains of varying lengths and sequences. *J. Biol. Chem.* **281**, 28033-28038 (2006)
21. Saio,T., Guan,X., Rossi,P., Economou,A. & Kalodimos,C.G. Structural basis for protein antiaggregation activity of the trigger factor chaperone. *Science* **344**, 1250494 (2014)
22. Hsu,S-T.D. *et al.* Structure and dynamics of a ribosome-bound nascent chain by NMR spectroscopy. *PNAS* **104**, 16516-16521 (2007)
23. Rutkowska,A. *et al.* Large-scale purification of ribosome-nascent chain complexes for biochemical and structural studies. *FEBS Lett.* **583**, 2407-2413 (2009)
24. Eichmann,C., Preissler,S., Riek,R., & Deuerling,E. Cotranslational structure acquisition of nascent polypeptides monitored by NMR. *PNAS* **107**, 9111-9116 (2010)
25. Christodoulou,J. *et al.* Heteronuclear NMR investigations of dynamic regions of intact *E. coli* ribosomes. *PNAS* **101**, 10949-10954 (2004)
26. Elcock,A.H. Molecular simulations of cotranslational protein folding: fragment stabilities, folding cooperativity, and trapping in the ribosome. *PLOS Comp Biol* **2**, e98 (2006)
27. O'Brien,E.P., Christodoulou,J., Vendruscolo,M. & Dobson,C.M. Trigger factor slows co-translational folding through kinetic trapping while sterically protecting the nascent chain from aberrant cytosolic interactions. *JACS* **134**, 10920-10932 (2012)
28. Ingólfson,H.I. *et al.* The power of coarse graining in biomolecular simulations. *Wires. Comput. Mol. Sci.* **4**, 225-248 (2014)
29. Dedmon,M.M., Lindorff-Larsen,K., Christodoulou,J., Vendruscolo,M. & Dobson,C.M. Mapping long-range interactions in α-synuclein using spin-label NMR and ensemble molecular dynamics simulations *JACS.* **127**, 476-477 (2005)
30. Li,C. *et al*. Differential dynamical effects of macromolecular crowding on an intrinsically disordered protein and a globular protein: implications for in-cell NMR spectroscopy. *JACS.* **130**, 6310-6311 (2008)
31. Waudby,C.A. *et al.* In-cell NMR characterization of the secondary structure populations of a disordered conformation of α-Synuclein within *E. coli* cells. *PLOS One* **8**, e72286 (2013)
32. Nakatogawa,H. & Koreaki, I. Secretion monitor, SecM, undergoes self-translation arrest in the cytosol. *Mol. Cell* **7**, 185-192 (2001)

33. Cabrita,L.D. *et al.* Probing ribosome-nascent chain complexes produced *in vivo* by NMR spectroscopy. *PNAS* **106**, 22239-22244 (2009)
34. Schanda,P. *et al.* Very fast two-dimensional NMR spectroscopy for real-time investigation of dynamic events in proteins on the time scale of seconds. *JACS* **127**, 8014-8015 (2005)
35. Waudby,C.A. *et al.* An analysis of NMR sensitivity enhancements obtained using non-uniform weighted sampling, and the application to protein NMR. *J. Mag. Res.* **219**, 46-52 (2012)
36. Kirchdoerfer,R.N., Huang,J.J.-T., Isola,M.K. & Cavagnero,S. Fluorescence-based analysis of aminoacyl- and peptidyl-tRNA by low-pH sodium dodecyl sulfate- polyacrylamide gel electrophoresis. *Anal. Biochem.* **364**, 92-94 (2007)
37. Ferrage,F. *et al.* Slow diffusion of macromolecular assemblies by a new pulsed field gradient NMR method. *JACS.* **125**, 2541-2545 (2003)
38. Amand,B., Pochon,F. & Lavalette,D. Rotational diffusion of *Escherichia coli* ribosomes. I. –Free 70S, 50S and 30S particles. *Biochimie* **59**, 779-784 (1977)
39. Tomic,S., Johnson,A.E., Hartl,F.U. & Etchells,S.A. Exploring the capacity of trigger factor to function as a shield for ribosome bound polypeptide chains. *FEBS Lett.* **580**, 72-76 (2006)
40. Lakshmipathy,S.K., Gupta,R., Pinkert,S., Etchells,S.A., Hartl,F.U. Versatility of trigger factor interactions with ribosome-nascent chain complexes. *J. Biol. Chem.* **285**, 27911-27923 (2010)
41. Banavar,J.R. *et al.* Physics of proteins. *Ann.Rev.Biop.Biomol.Struc.* **36**, 261-280 (2007)
42. Bhushan,S. *et al.* SecM-stalled ribosomes adopt an altered geometry at the peptidyl transferase center. *PLOS Biol* **9**, e1000581 (2011)
43. Sandikci,A. *et al.* Dynamic enzyme docking to the ribosome coordinates N-terminal processing with polypeptide folding. *NSMB.* **20**, 843-849 (2013)
44. Papoian,G.A. Proteins with weakly funneled energy landscapes challenge the classical structure-function paradigm. *PNAS* **105**, 14237-14238 (2008)
45. Camilloni,C. *et al.* A relationship between the aggregation rates of α Syn variants and the β -sheet populations in their monomeric forms. *J Phys Chem B* **117,** 10737–10741 (2013)

46. Bah,A. *et al.* Folding of an intrinsically disordered protein by phosphorylation as a regulatory switch. *Nature* **519**, 106-109 (2015)
47. Deleersnijder,A., Gerard,M., Debyser,Z. & Baekelandt,V. The remarkable conformational plasticity of alpha-synuclein:blessing or curse? *Trends Mol. Med.* **19**, 368-377 (2013)
48. Theillet,F.X. *et al.* Structural disorder of monomeric α-synuclein persists in mammalian cells. *Nature* **530**, 45-50 (2016)
49. Merz,F. *et al.* Molecular mechanism and structure of trigger factor bound to the translating ribosome. *EMBO J.* **27**, 1622-1632 (2008)
50. Brandt,F. *et al.* The native 3D organization of bacterial polysomes. *Cell* **136**, 261-271 (2009)
51. Gumbart,J., Schreiner,E., Wilson,D.N., Beckmann,R. & Schulten,K. Mechanisms of SecM-mediated stalling in the ribosome. *Biophys. J.* **103**, 331-341 (2012)
52. Pronk,S. *et al.* GROMACS 4.5: a high-throughput and highly parallel open source molecular simulation toolkit. *Bioinformatics* **29**, 845-854 (2013)
53. Sivashanmugam, A. *et al.* Practical protocols for production of very high yields of recombinant proteins using *Escherichia coli*. *Prot. Sci.* **18**, 936-948 (2009)
54. Best,R.B., de Sancho,D. & Mittal,J. Residue-specific α-helix propensities from molecular simulation. *Biophys. J.* **102**, 1462-1467 (2012)
55. Betancourt,M.R. & Thirumalai,D. Pair potentials for protein folding: choice of reference states and sensitivity of predicted native states to variations in the interaction schemes. *Protein Sci.* **8**, 361-369 (1999)
56. Ernst,R.R., Bodenhausen,G. & Wokaun,A. Principles of nuclear magnetic resonance in one and two dimensions. *Oxford University Press*, New York (1987)
57. Johnson,E. *et al.* A multifaceted approach to the interpretation of NMR order parameters: A case study of a dynamic α-helix. *J. Phys. Chem. B.* **112**, 6203-6210 (2008)
58. Koppel,D.E. Study of *Escherichia coli* ribosomes by intensity fluctuation spectroscopy of scattered laser light. *Biochemistry* **13**, 2712-2719 (1974)

FIGURES

Figure 1:

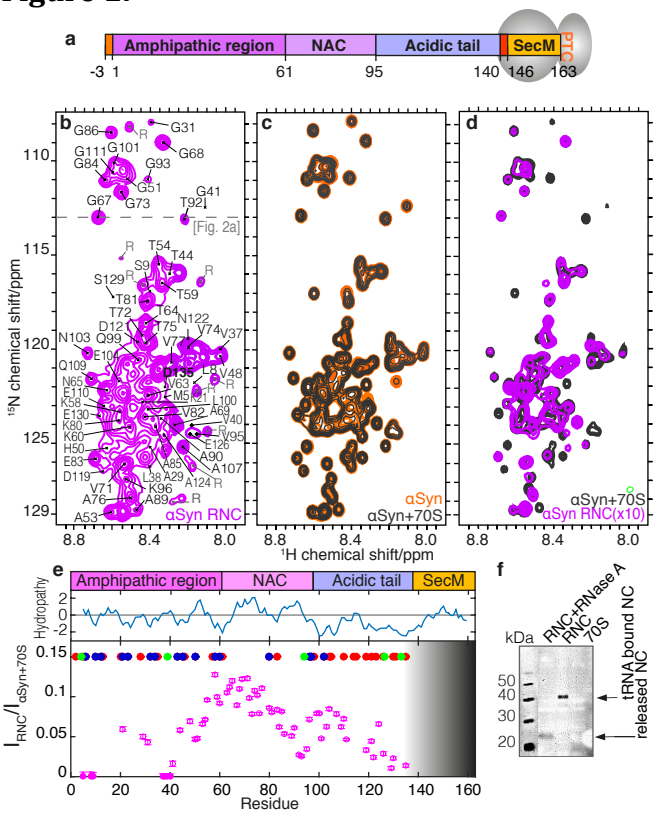

Figure 1: NMR characterization of the αSyn RNC (a) Schematic of the αSyn RNC construct. **(b)**^{1}H-^{15}N SOFAST-HMQC spectrum of the αSyn RNC and resonance assignments; R indicates 70S background peaks. **(c)**Comparison of ^{1}H-^{15}N SOFAST-HMQC spectra of isolated αSyn with & without 1 mol. equiv. of ribosomes. **(d)**Comparison of the αSyn RNC spectra in(b)&(c) with RNC intensities amplified. **(e)**Cross-peak intensities in αSyn RNC relative to isolated αSyn in the presence of ribosomes, the grey shaded area depicts the approximate length of the exit tunnel. A Kyte & Doolittle hydropathy plot and an amino acid classification of the αSyn protein sequence in positively charged(blue), negatively charged(red) and aromatic(green) residues is also shown. **(f)**Anti-SecM western blot to probe for RNC integrity, showing tRNA-bound(~40kDa) and released αSyn NCs(~20kDa).

Figure 2:

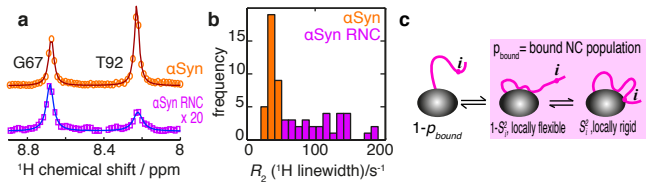

Figure 2: ^{1}H linewidth analysis of the αSyn RNC. **(a)**^{1}H cross-sections through ^{1}H-^{15}N SOFAST-HMQC spectra(δ_N113.15ppm,Fig.1b,dashed line) of isolated αSyn and the αSyn RNC fitted to a sum of Lorentzian functions(solid lines) to determine ^{1}H R_2 rates. **(b)**Distribution of R_2 values obtained from lineshape fitting of residues selected from V48-A124 for isolated αSyn(34 residues) and αSyn RNC(31 residues). **(c)**Schematic depicting the exchange of the NC between its free and ribosome-associated states. The globally bound state consists of a population-weighted average of a locally flexible state, where residue *i* is highly dynamic but in close proximity to residues tethered nearby, and a locally rigid state with residue *i* being in direct contact with the ribosome surface. The relative proportions of these states are described by the generalised order parameter, S^2.

Figure 3:

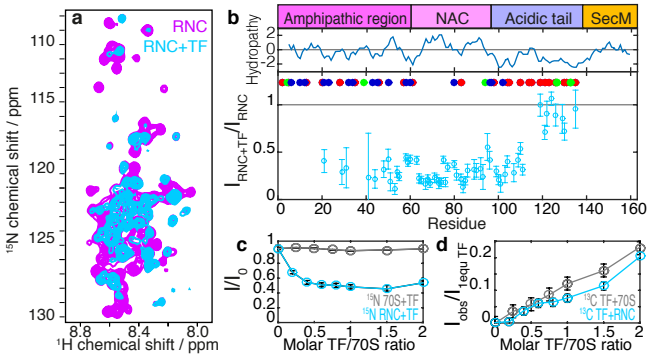

Figure 3: NMR analysis of the interaction of trigger factor with αSyn RNCs. **(a)**Comparison of ^{1}H-^{15}N SOFAST-HMQC spectra of the αSyn RNC with & without 1 mol. equiv. TF. **(b)**Relative cross-peak intensities of the αSyn RNC following addition of TF. A Kyte & Doolittle hydropathy plot and an amino acid classification of the αSyn protein sequence in positively charged(blue), negatively charged(red) and aromatic(green) residues is shown. **(c)**Changes in the integrals of ^{15}N-edited ^{1}H amide envelopes of the αSyn RNC and ^{15}N-labelled 70S ribosomes with increasing TF. **(d)**Changes in the integrals of ^{13}C-edited ^{1}H methyl envelopes with increasing TF, in the presence of αSyn RNC(6.5μM 70S) and 70S ribosomes(5μM 70S). Integrals have been

normalized to a 10μM sample of isolated TF scaled according to the 70S concentration(neglecting effects of the TF monomer/dimer equilibrium).\

Figure 4:

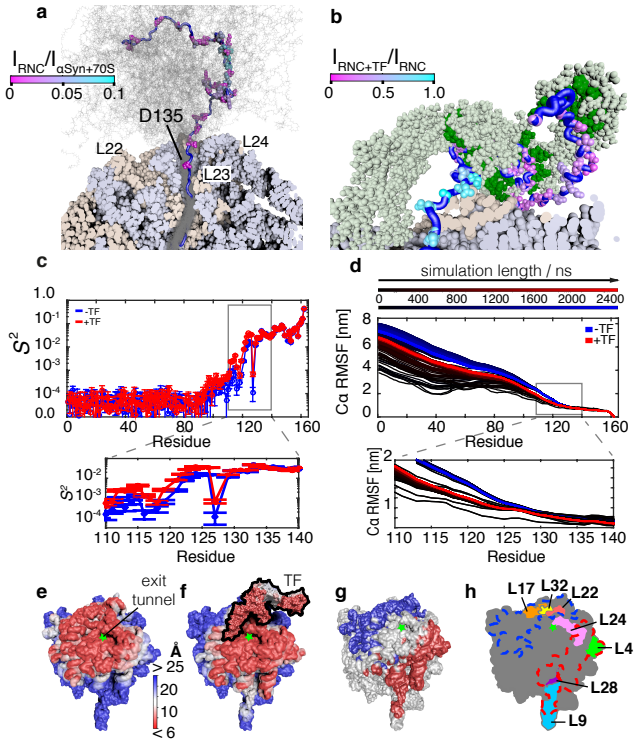

Figure 4: Structural modeling of the αSyn RNC. (a) Cross-section of the simulated αSyn RNC showing the NC ensemble(grey) with a representative NC structure highlighted(blue), ribosomal proteins(beige) & RNA(blue-grey). Observed NMR resonances(relative to isolated αSyn in the presence of 70S,Fig.1e) are shown as spheres colored according to their relative intensity(Fig.1e). **(b)**αSyn RNC model with TF monomer(light green), substrate binding pockets[21](dark green), the observed NC resonances are shown as spheres colored according to the relative intensity in Fig.3b; for clarity, residues 1–31 are not shown. **(c)**Amide S^2 order parameters determined from simulated ensembles with & without TF. **(d)**Cα RMSF of the αSyn RNC calculated over increasing lengths of the simulation trajectory, with & without TF. **(e)**Ribosome surface colored according to the distance of closest approach of the simulated NCs and **(f)**ribosome and TF surfaces colored as described in(e). **(g)**Difference in ribosome surface accessibility(distance of closest approach) on TF binding. Blue Regions become sterically restricted, whereas red regions represent parts of the ribosome surface that are more frequently contacted by the NC due to the steric restrictions imposed by TF on other parts of the

ribosome surface. **(h)**Schematic diagram of ribosomal proteins in close proximity to the exit tunnel; ribosome orientation as in(e–g).

Supplementary Information

Structural characterization of the interaction of α-synuclein nascent chains with the ribosomal surface and trigger factor

Deckert *et al.*

Materials & Methods

List of Supplementary Figures:

Supplementary Materials:

Materials & Methods

Preparation of αSyn RNCs and 70S ribosomes from *E.coli*. Uniformly ^{15}N-labelled RNCs were overexpressed in *E.coli* using enhanced minimal media (EM9), adapted from Sivashanmugam *et al*[53] and purified as described previously[33]. During purification, the RNCs were isolated using Ni^{2+} affinity chromatography and TEV protease was used to remove the H_6-tag, prior to sucrose density ultracentrifugation. The purified RNC samples were concentrated and buffer exchanged into Tico Buffer (10mM Hepes, 30mM NH_4Cl, 12mM $MgCl_2$, 5mM EDTA, 2mM BME, pH 7.0) to 300µl for NMR spectroscopy. ^{15}N-labelled 70S ribosomes were prepared in a similar manner to the RNC samples with the omission of both the affinity chromatography and TEV protease cleavage steps. Unlabeled 70S ribosomes were prepared from *E.coli* cultures grown in LB medium. The concentration of 70S ribosomes was calculated using $1Abs_{260}$=24pmol.

Detection and integrity of RNCs. RNC samples are collected during purification or NMR acquisition at regular intervals and run on bis-tris polyacrylamide gels (pH 5.8) prior to immunodetection by western blot, using enhanced chemiluminescence. The low pH conditions of the polyacrylamide gels retains the ester bond between the last incorporated amino acid and the tRNA[36], such that the tRNA-bound RNCs migrate with an additional ~25kDa (mass tRNA). The released αSyn NC has a calculated molecular weight of ~18kDa (ExPASy ProtParam) but migrates with an apparent MW of ~20kDa. Western blot and ^{15}N diffusion (see below) were used in tandem to determine the lifetime of the sample, to ensure NMR analysis reflected only intact RNC species. NC occupancy was determined by western blot analysis using isolated αSyn as a standard for protein concentration. ^{15}N-edited and ^{15}N-filtered ^{1}H 1D experiments were used to determine the extent of ribosomal background, which was calculated to be less than 5% across all samples.

Preparation of trigger factor. TF was expressed in deuterated EM9 media supplemented with metabolic precursors, which were selectively protonated at methyl groups for isoleucine (2-Ketobutyric acid-4-^{13}C, 3-d_2 (Sigma-Aldrich), leucine and valine (2-Keto-3(methyl-d_3)-butyric acid-4-^{13}C, 3-d_1 (Sigma-Aldrich) for selective methyl labeling. Following lysis, the TF proteins were purified using Ni-NTA chromatography, followed by H_6-tag removal using TEV protease and size exclusion chromatography. Pure TF was concentrated and buffer exchanged into Tico buffer.

NMR spectroscopy. NMR data were acquired for the αSyn RNC at 16.4T (700MHz) at 277K using a Bruker Avance III spectrometer (Bruker BioSpin, Karlsruhe, Germany) equipped with a TXI cryoprobe. ^{1}H-^{15}N SOFAST-HMQC[34] spectra of the αSyn RNC were recorded using non-uniform weighted sampling methods[35] with 1024 complex points and a sweep width of 10504Hz in the direct (^{1}H) dimension, and 122 complex points and a sweep width of 1845Hz in the indirect (^{15}N) dimension with a recycle time of 50ms. ^{15}N-edited X-STE diffusion measurements[37] were recorded by using a diffusion delay of 100ms, and bipolar trapezoidal gradient encoding pulses of a total length of 4ms and strengths corresponding to 5% (0.028Tm^{-1}) and 95% (0.532Tm^{-1}) of the maximum gradient strength (0.56Tm^{-1}). The SOFAST-HMQC and X-STE measurements were carried out in an interleaved manner, allowing the integrity of the RNC to be continuously ascertained. NMR data was processed and analyzed by NMRPipe and Sparky software packages.

^{1}H linewidth analysis. ^{1}H cross-sections of ^{1}H-^{15}N SOFAST-HMQC spectra of isolated αSyn and the αSyn RNC Spectra were processed with 12Hz exponential apodization and fitted to a sum of Lorentzian functions to determine ^{1}H R_2 rates.

TF titration and analysis. ^{15}N- and ^{13}C-edited 1D envelopes were recorded for the RNC, prior to the addition of TF to the samples. The different labeling schemes permitted the monitoring of the ^{15}N-labelled αSyn NC as well as the ^{2}H-TF that was selectively ^{13}C-labelled and protonated at all Ile, Leu and Val side chain methyl groups. The ribosome concentration (Ab_{260}) measured for the RNC was 6.5μM with a NC occupancy of 62% (i.e. NC concentration was 4.0±0.4μM). TF was added according to the ribosome concentration starting with 0.2 equivalents up to 0.4, 0.6, 0.8, 1, 1.5, 2, and 3 molar equivalents. Experiments were repeated in a similar manner (with 0.25, 0.5, 0.75, 1, 1.5, 2 and 5 molar equivalents of TF) for the interaction of TF with unoccupied 70S ribosomes at 5μM concentration. For analysis, the integrals of the amide (or methyl) envelope was determined and normalized relative to a sample of isolated TF (10μM). These were subsequently scaled according to the ribosome concentration for comparative analysis with RNCs. In these measurements, the contributions arising from the TF monomer/dimer equilibrium were considered to be minimal and thus were not included in the analysis.

Modeling of the *E.coli* 70S stalled with an αSyn NC. An atomic model of a stalled NC on the ribosome was derived from cryo-electron microscopy data[42] by molecular-dynamics flexible fitting[51]. The original NC sequence in the model was replaced and extended to the sequence of

the αSyn RNC using Swiss-PDB Viewer. TF bound to ribosome was modeled based on the cryo-electron microscopy data of the ribosome-TF complex[49] and the atomic structure of TF[14,15]. The NC mobility for each residue was calculated as root mean square fluctuations (RMSF) from the average position of CA atoms within the trajectory.

Coarse-grained MD simulations of the αSyn RNC in the presence and absence of TF. Coarse-grained simulations of the αSyn RNC were performed using a version of the tube model[41], known as the CamTube force field, which was implemented in Gromacs[52] via tabulated potentials. Each amino acid is represented by its five backbone atoms (N, H, CA, C and O) and one atom (CB) has been used to model side-chains with the length of the CA-CB bond being amino acid-dependent. The bonded interactions are taken from the Amber force field[54]. The tube-like behavior is obtained by imposing a hard sphere potential on all the atoms. In addition, hydrogen bonding is modelled as Lennard-Jones interactions between pairs of O and H atoms, whereas hydrophobic and electrostatic interactions are introduced by residue-specific contact potentials implemented only between CB atoms of the residue pairs using the square well function. These potentials are adapted from lattice models of protein folding and parameterized based on the contact frequencies between amino acid pairs in the PDB[55]. Additionally a curvature penalty was introduced into the CamTube force field in form of a weak repulsive force between C and H atoms that are separated by two or three residues along the protein chain. Amber force field parameters were changed for CB-CA-N-C and CB-CA-C-N dihedral angles in order to reproduce correct Ramachandran plots in the CamTube force field. Within the CamTube model, the ribosome and TF are represented as frozen hard spheres with a 5Å radius centered on P and CA carbon atoms for RNA and protein molecules, respectively. The system was simulated using a stochastic dynamics algorithm with a time step of 2fs together with the LINCS algorithm to constrain bond lengths. In order to enhance the NC sampling of the available space all simulations were performed at 345K and run for 2.4μs. For analysis we calculated the minimum distance between the CA atoms of the NC and the CA and P atoms of the ribosomal surface within 6 distance ranges (<6, 10, 15, 20, 25, >25) for which the ribosome surface was colored accordingly.

Analysis of the MD trajectory. Estimates of ^{1}H R_2 relaxation rates for a rigid bound state were calculated, as an ensemble average of 50 all-atom RNC structures, from the sum of ^{1}H-^{1}H dipolar interactions[56]:

$$R_{2,i} = \langle \sum_{j \in H\ atoms} \frac{1}{5} \left(\frac{\mu_0}{4\pi}\right)^2 \frac{\hbar^2 \gamma_H^4 S_{ij}^2 \tau_c}{r_{ij}^6} \rangle \quad (1)$$

where γ_H is the proton gyromagnetic ratio, $S_{ij}^2 = 1$ are the generalised order parameters for internuclear bond vectors, and $\tau_c = 3.9\mu s$ is the ribosome rotational correlation time at 277K in H_2O[38] . Only the zero frequency spectral density has been considered, as given the slow tumbling of the ribosome the contribution from higher frequency terms is negligible.

Amide S^2 generalised order parameters were calculated from an ensemble of 8000 all-atom RNC structures, where θ and ϕ are angles of the N-H bond vector relative to the fixed molecular reference frame[57]:

$$S^2 = \frac{4\pi}{5} \sum_{m=-2}^{2} \langle Y_{2m}(\theta, \phi) \rangle \langle Y_{2m}^*(\theta, \phi) \rangle \quad (2)$$

Figure S1:

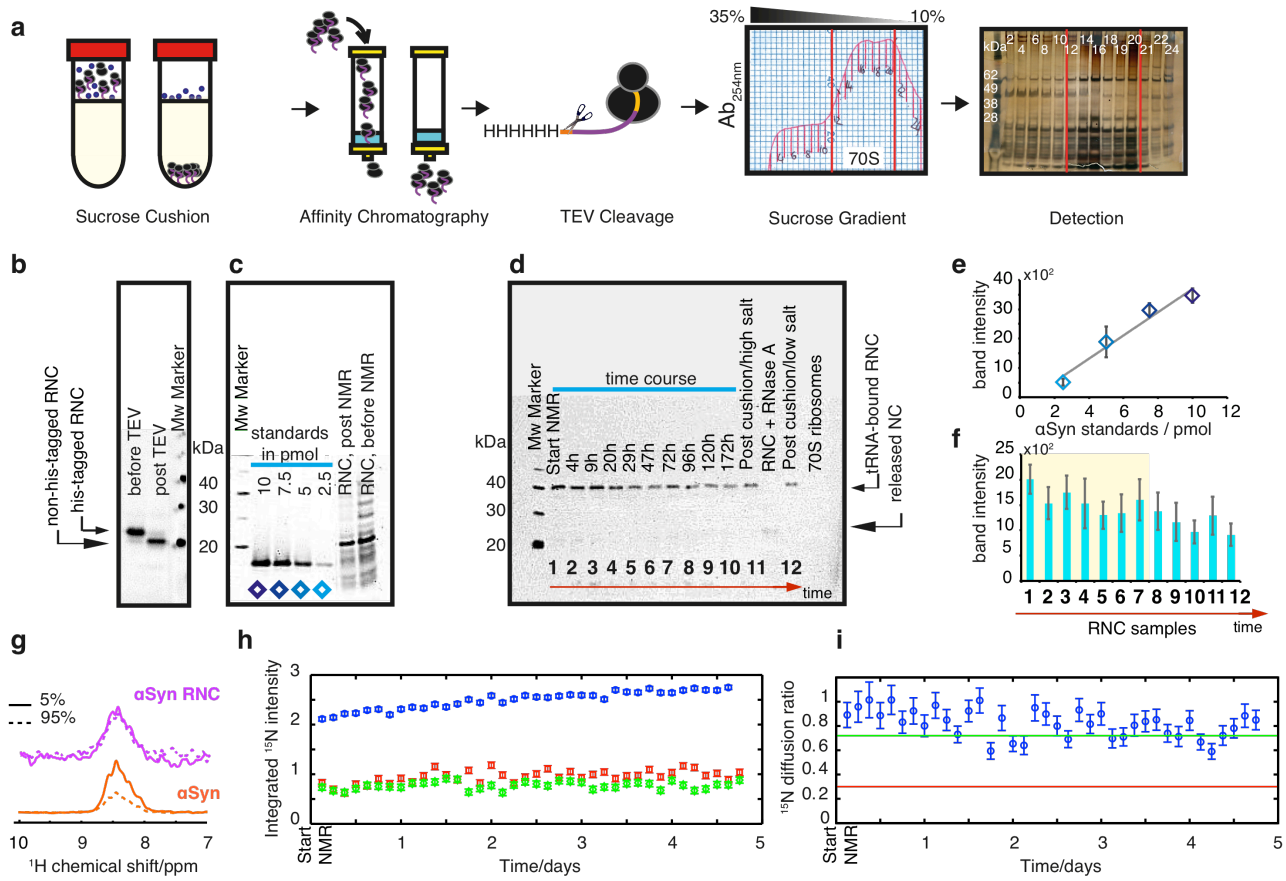

Figure S1: RNC purification and monitoring of sample stability of ^{15}N-labelled αSyn RNCs

(a) αSyn RNC purification involves a four-stage strategy including: a sucrose cushion to pellet ribosomal material, nickel affinity chromatography to selectively enrich NC occupied ribosomes using the N-terminal H_6-tag, purification tag removal using a TEV protease and a sucrose gradient ultracentrifugation step. 70S-containing fractions (indicated by red borders) were identified using absorbance measurements at 254nm and silver staining of SDS-PAGE. **(b)** Anti-SecM western blot of samples (10pmol) collected during RNC purification. A band shift of ~0.6kDa is observed in the NC following TEV cleavage to remove H_6-tag (lane 1 to lane 2). **(c)** Ribosome occupancy determination: anti-αSyn western blot RNC sample (10pmol, 70S ribosome concentration) relative to αSyn protein standards. **(d)** Anti-SecM western blot of the RNC sample during its NMR acquisition period. The band at ~40kDa is indicative of a tRNA-bound RNC species[36]. **(e)** NC occupancy as determined by western blot: Band intensities of isolated αSyn standards (from c) plotted against concentrations, alongside the corresponding calibration used for quantitative analysis. **(f)** NC integrity as assessed over time. Band

intensities of RNC samples loaded in (d) are plotted over time to monitor the integrity of the NC species over the course of NMR data acquisition. The timeframe during which the sample is deemed to be intact is highlighted in yellow. **(g)** ^{15}N-XSTE diffusion NMR measurements, at 5% and 95% gradient strengths as indicated, for an attached αSyn NC and isolated αSyn. **(h)** The integrated intensities of the ^{15}N-edited 1D envelope over time (blue circles) and ^{15}N-stimulated echo diffusion measurements[37] on the αSyn RNC at 5% (red squares) and 95% (green squares) of the maximum gradient strength. Error bars indicate the standard error of the mean derived from measurements of spectral noise. **(i)** Intensity ratio $I_{95\%}/I_{5\%}$ of the αSyn RNC during NMR data acquisition (average $I_{95\%}/I_{5\%}$ ~0.82 ± 0.12 and D=7.67±5.56x10^{-12} m^{2}s^{-1}). The green line represents the intensity ratio measured for intact 70S ribosomes (hydrodynamic radius r_h = 12.6nm[58], diffusion coefficient D=1.1x10^{-11} m^{2}s^{-1} at 277K in H_2O). The red line indicates the intensity ratio of isolated αSyn (r_h = 2.72 nm[29], D = 5x10^{-11} m^{2}s^{-1} at 277K in H_2O).

Figure S2:

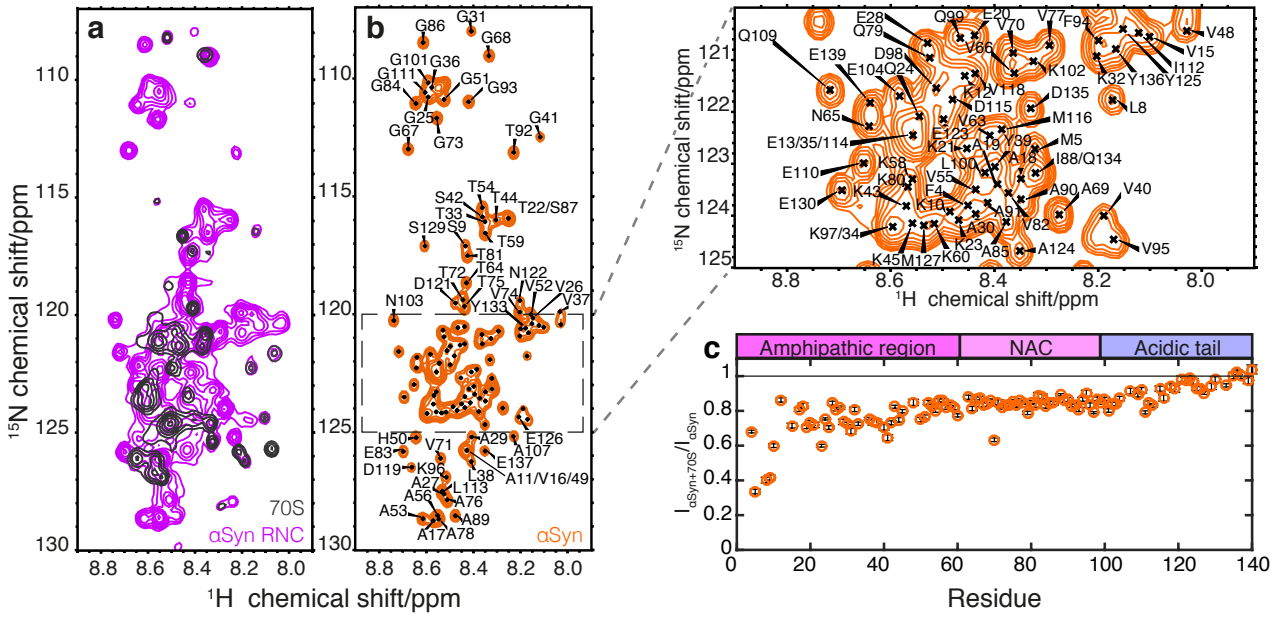

Figure S2: NMR experiments of 70S ribosomes and isolated αSyn

NMR experiments of isolated αSyn in the presence of 70S ribosome, recorded under the same conditions as the αSyn RNC sample (277K in Tico buffer at pH 7.0). **(a)** Overlay of ^{1}H-^{15}N SOFAST-HMQC spectrum of the αSyn RNC in magenta with the ^{1}H-^{15}N SOFAST-HMQC spectrum of ^{15}N-labeled 70S ribosomes (dark grey). The ribosome spectrum was recorded to identify potential ribosomal peaks in the αSyn RNC spectrum originating from background labeling of the ribosomal protein L7/L12[26] (dark grey). **(b)** ^{1}H-^{15}N SOFAST HMQC spectrum of isolated αSyn with backbone assignment. Boxed area in (b) expanded for clarification. **(c)** Relative cross-peak intensities of WT αSyn (orange) in the presence and absence of 1 molar equivalence 70S ribosomes.

Figure S3:

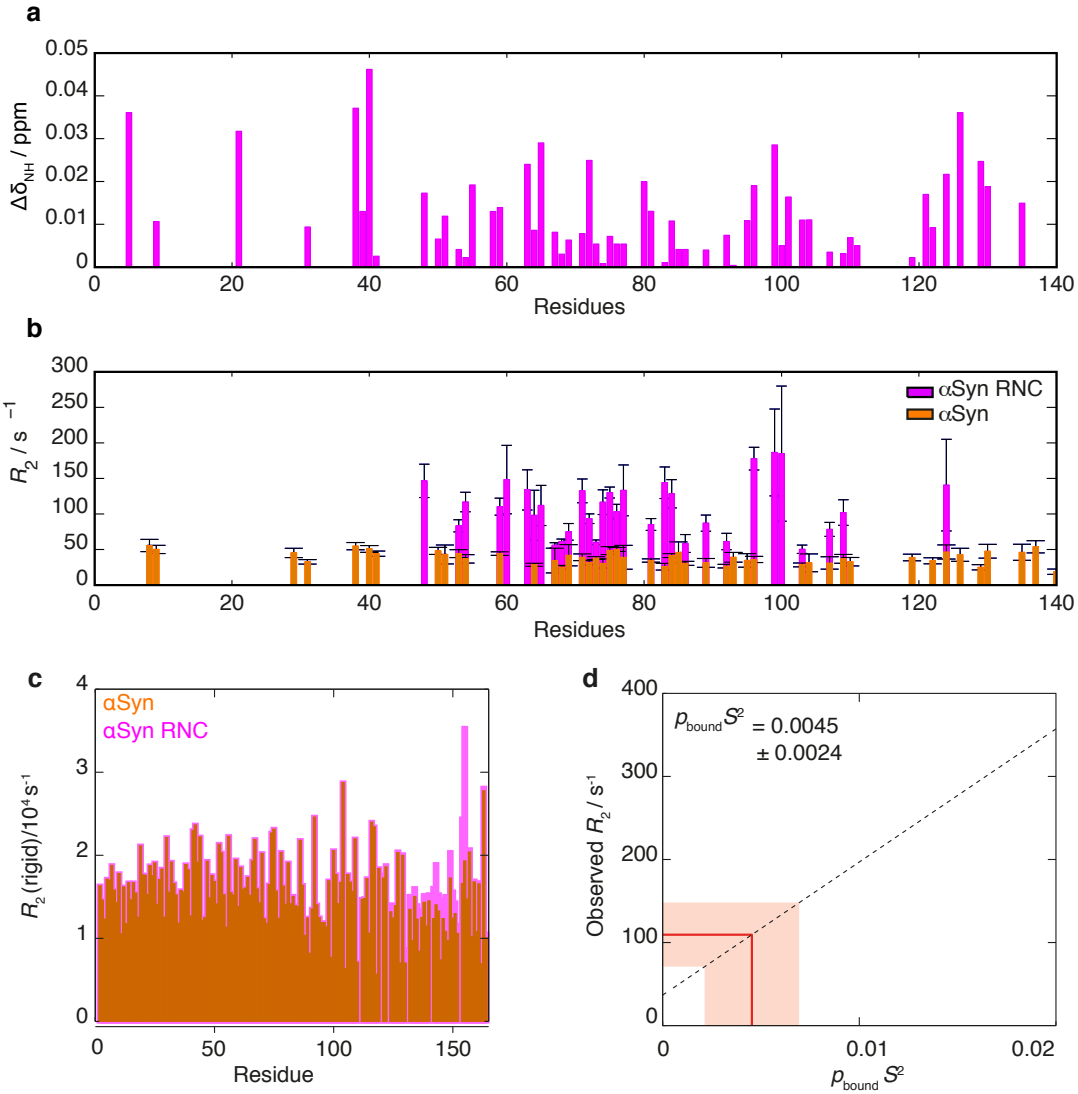

Figure S3: Chemical shift changes and lineshape analysis for the αSyn RNC & isolated αSyn

(a) $\Delta\delta_{NH}$ chemical shift changes between the isolated αSyn protein and the αSyn RNC ($\Delta\delta_{NH} = [\Delta\delta_H^2+(\Delta\delta_N/5)^2]^{½}$). **(b)** Transverse relaxation rate (R_2) determined for αSyn bound to the ribosome (magenta) and αSyn in isolation (orange). R_2 values were resolved by fitting the NMR resonances to Lorentzian lineshapes. Since $^3J_{HNHA}$ couplings were not resolved, we note that these relaxation rates are expected to contain an additional contribution of ca. 20-30s^{-1} (6-10Hz). **(c)** ^{1}H amide linewidths estimated for a rigid ribosome-associated state by averaging of ^{1}H-^{1}H dipolar interactions across an ensemble of all-atom models of the αSyn RNC. Calculations were repeated to both include (magenta) and exclude (orange) the effect of ribosomal protons. **(d)** Estimation of ribosome-bound populations of αSyn RNC using measured linewidths of free αSyn (Fig. 2b) and calculated bound-state linewidths (Fig. 2c), $R_{2,obs} = R_{2,free} + p_{bound}S^2R_{2,rigid}$

(black dashed line). The red line and shaded area shows the mean ± s.d. of linewidths measured for the αSyn RNC (residues 48 to 124), and the associated bound-state population.

Figure S4:

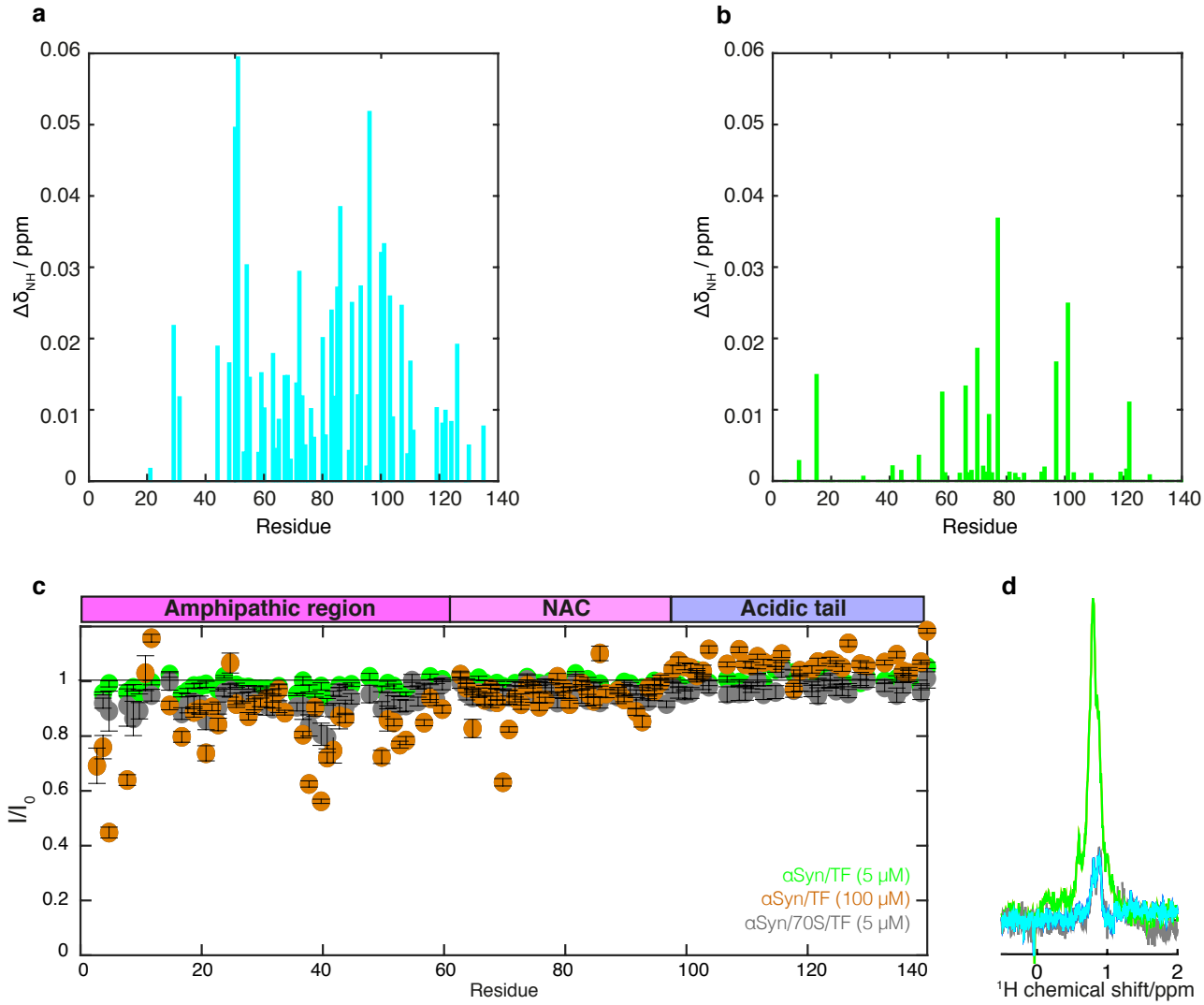

Figure S4: Chemical shift and peak intensity perturbations of isolated αSyn and the αSyn RNC upon addition of TF

(a) ΔNH chemical shift changes between the αSyn RNC in the presence and absence of TF and **(b)** between isolated αSyn in the presence and absence of TF. **(c)** Relative cross-peak intensities between isolated αSyn in the presence of both 70S ribosomes and TF compared to αSyn+70S only (grey circles), between αSyn+TF compared to isolated αSyn at 5μM (green circles) and 100μM (orange circles) equivalent concentrations. **(d)** ^{13}C-edited 1D envelopes of 10μM TF (green), in the presence of the αSyn RNC (blue) and the presence of 70S ribosomes (grey)

Figure S5:

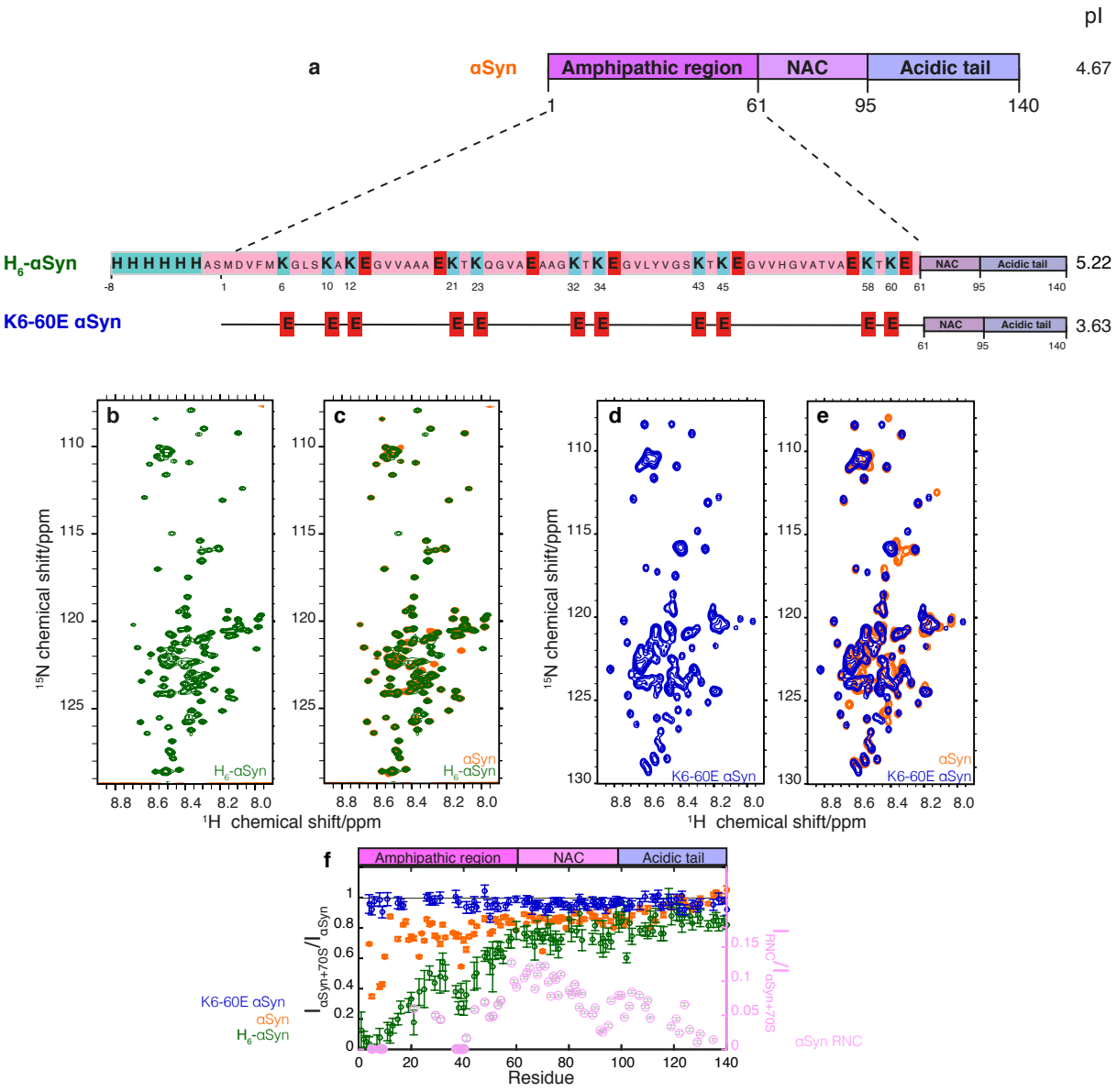

Figure S5: NMR spectra and relative cross-peak intensities of the αSyn charge variants

(a) Charge variants constructed to investigate the effect of electrostatics. Of the 15 Lys residues within the αSyn sequence, the first 11 (residue K6 to K60) were mutated to Glu, lowering the pI from 4.67 (WT) to 3.63 (K6-60E). Having an N-terminal hexa-histidine (H_6) tag increased the pI to 5.22. **(b)** ^{1}H-^{15}N HSQC spectrum of H_6-αSyn (green) and in **(c)** overlaid with WT αSyn (orange). **(d)** ^{1}H-^{15}N SOFAST HMQC spectrum of K6-60E αSyn (blue) and in **(e)** overlaid with WT αSyn (orange). **(f)** Relative cross-peak intensities of K6-60E αSyn (blue), WT αSyn (orange, as in Fig. S2c) and H_6-αSyn (green) in the presence and absence of 1molar equivalence 70S

ribosomes. Cross-peak intensities in αSyn RNC relative to isolated αSyn in the presence of ribosomes (pink, as in Fig. 1e) have been plotted again for better comparison between the line broadenings observed in the N-terminal region of the RNC as well as isolated αSyn.